UNIVERSITY OF CAMBRIDGE
Department of Engineering

THE INTERACTION OF WATER WAVES AND POROUS MEDIA

Author Name: Warinthorn Angkanasirikul

Supervisor: Dr. Dongfang Liang

Date: 27 May 2020

I hereby declare that, except where specifically indicated, the work submitted herein is my own original work.

Signed วรินทร์ธร อังคณาสิริกุล *date* 27 May 2020

Technical abstract

Water-soil interaction has been a challenge for investigating hydraulic problems such as overtopping induced dam failures and the erosion of riverbanks and coastal areas where water waves can easily become hydrological or meteorological disasters. This can cause a threat to human life and lead to significant economic losses. Therefore, flood defences that could potentially stop or slow down the invasion of free surface flows have become increasingly vital infrastructure due to population growth and climate change, particularly in response to continually rising global sea levels.

Using numerical simulation is more cost-effective than using physical experiments even on a small scale. The material point method (MPM) was first introduced in the analysis of large deformation problems in solid mechanics. Since the background mesh is used only for solving balance equations while the material properties are stored on the material points, mesh distortions exhibited in the classical finite element method are easily avoided when coping with large deformations. With dual sets of material points representing the solid phase and the liquid phase separately, the two-point MPM is capable of capturing the relative movement between water and solid skeletons

In this research, a porous media is investigated via two-point MPM. The capability of the porous media to absorb wave energy is an interest in coastal engineering. In addition, as the flow friction developing within the porous media can be exploited to create significant wave energy dissipation. In order to verify the accuracy of the MPM, simulations of dam-break flows are carried out and the results are in good agreement with the experimental data and other validated numerical methods and. Furthermore, simulations of the model from Liu et al.'s paper (1999) are investigated, and the results are also in good agreement with the experimental data obtained. Therefore, MPM is considered to be the most suitable method for this investigation.

There are three key factors related to the porous media that are investigated in this study (Height, Porosity and Grain size). In terms of height of the porous media (H'), it is shown that the taller the porous media is, the slower the water can travel through the barrier. The reasons to explain this phenomenon are, for example, there are more spaces within the structure that can contain more water particles, so the water particles take more time to travel to the other

side of the porous structure when compared to the speed of the overtopping water and the amount of the reflected water at the barrier is greater with a higher media, thereby easing some portion of the water to reach the end of the flume. In addition, there are two distinct trends when the graph of the front flood position against time is considered (one is roughly parallel with the trend without porous structure and the other is not), so, for the next two factors, one height from each trend is investigated, $\mathrm{H}' = 0.07$ m and $\mathrm{H}' = 0.15$ m.

For the investigation of effect of porosity, there are four values included in the study which are 0.50, 0.70, 0.80 and 0.95 in both of the height. They both show that the greater value of porosity the porous barrier has, the faster the speed of water travels through the structure. Moreover, when consider the graph of speed of water propagating through the porous media against porosity value, it is demonstrated that both of the heights have similar trends.

In the study of impact of grain size, there are five values included in this investigation which are 5 mm, 10 mm, 30 mm, 50mm and 100mm in both of the heights. They both show that the greater value of grain size the porous barrier has, the faster the speed of water travels through the structure. This means that it is easier for water to travel through the porous media with a greater grain size since the total distance for water to travel is lower. When the graph of the speed of water propagating through the porous media against the grain size is deemed, there is no clear trend between those two height values. Between approximately 23 mm and 65 mm, the speed of water from $\mathrm{H}' = 0.15$ m is greater than that from $\mathrm{H}' = 0.07$ m. However, this exception might apply to only this model.

In terms of the further study, the wave column on the left-hand side of the flume can be changed into a set of stationary waves, which might produce more realistic results when compared to the real-world scenarios. Furthermore, by placing the porous media, it is on a small-angle slope would make it more realistic.

Nomenclature

$\boldsymbol{a}$	Acceleration (m/s^2)
$\boldsymbol{b}$	Specific body force (m/s^2)
$\boldsymbol{f_d}$	Drag force
$\boldsymbol{g}$	Gravitational field strength (m/s^2)
0	Subscript index indicating some reference value
D	Grain size
H'	Height of porous media
K	Bulk modulus (kPa)
M_p	Mass of material point
n	Soil porosity
N_n	Number of nodes
N_p	Number of material points
p	Pressure (kPa)
x	Horizontal co-ordinate (positive right)
x_p	Position of material point
Ω	Material domain
ρ	density (kg/m^3)
θ	Time scale
σ	Cauchy stress tensor
τ	Shear stress
κ	Permeability (m^2)
FEM	Finite Element Method
FLIP	Fluid Implicit Particle
MP	Material point
MPM	Material Point Method
PIC	Particle-in-cell
RVE	Representative Volume Element
SPH	Smoothed Particle Hydrodynamics
SWEs	Shallow Water Equations
VOF	Volume of Fluid

Table of Contents

Acknowledgements

First of all, I would like to express my thanks of gratitude to my supervisor, Dr. Dongfang Liang who has given me this opportunity to carry out the research and mentored me throughout this journey. I would also like to extend my gratitude to Dr. Xuanyu Zhao, Lucy Harris, and Grace Robert who have generously offered me support and guidance.

Special thanks to Issy Hanna and Karnthida Marem, with whom I have enjoyed fruitful discussion as well as developed precious friendship. Also, I would like to express my thanks to Joanna Ye and Shusma Balaji who have supported me academically and emotionally.

I am extremely grateful to my family who has believed in me and this research would never be possible without them.

Finally, the year of 2020 has been challenging to all of us as humanity. I would like to express my gratitude to all the people who reached out to me and supported me during this rollercoaster journey.

Chapter 1: Introduction

1.1 AIMS

Water-soil interaction has been a challenge for studying hydraulic problems such as the erosion of riverbanks and coastal areas and seepage flows through embankments. Numerical simulations are significantly less costly than physical experiments. This leads to the massive development of computer-aided simulation methods to investigate the interaction between soil and water over the past decades. This aim of study is to gain the in-depth understanding into water-coast interactions through the application of a numerical model and parametric studies, with a focus on propagation and dissipation processes.

1.2 COASTAL FLOOD DEFENCES

A seawall is an onshore coastal defence structure with the primary aim of protecting areas of human habitation or conservation from wave action, either because of normal tidal processes, or from extreme events resulting from storm surges.

Seawalls are typically large concrete structures. The simplest design is a vertical seawall built parallel to the coastal. This reinforces the existing coastal profile and reflects most of the wave energy. Porous coastal flood defences can also be implemented. These can range from human-engineered structures, such as rubble mounds, to more natural flood defences, such as sand dunes and vegetation. Natural flood barriers are much less visually intrusive and have demonstrated extreme effectiveness in flood protection. A report published by the United Nations Environment Program (UNEP) suggested that the Boxing Day tsunami in 2004 caused significantly less damage in the areas protected by natural barriers, such as mangroves, coral reefs or coastal vegetation.

1.3 THE EFFECTS OF CLIMATE CHANGE ON COASTAL FLOODING

Climate change refers to the long-term, large-scale change in the statistical distribution of weather patterns. This has increased both ocean temperatures and sea levels. This rise in sea temperatures and levels has a direct impact on the frequency and severity of extreme coastal weather events. With more frequent and severe floods driven by typhoons, hurricanes and cyclones, it is expected to have the design with additional height allowances for coastal defences on top of what has already been designed for.

1.4 INTRODUCTION TO MPM

The material point method (MPM) is a method between the particle-based methods and the Finite Element Method (FEM), used to simulate the behaviour of both solids and fluids. In MPM, the computational domain is spatially discretised in two frames. Firstly, the continuum body is divided into a group of material points (MPs). Each particle carries all the material variables: mass, velocity, stress, strain and position, which makes the MPM convenient for modelling based on history-dependent constitutive material points. Each point also has a constant mass but has a volume which can change. This enables compression or extension of material and then each MP moves with the body deformation. The mass and constitutive equations are solved at the MPs.

The latter frame is the computational mesh which is equivalent to a conventional finite element mesh and covers the full domain of the problem, including empty spaces in which particles may have to move into. The momentum equations are solved at the nodes of this computational mesh. The variables require to solve the governing equations for each of the calculation are transferred from the material points to the nodes of the mesh via mapping functions. Boundary conditions are imposed, either at the mesh nodes or at the MPs, and an incremental scheme is used to solve the governing equations. The quantities carried by the MPs are updated through the interpolation of the mesh results, via the same mapping function.

MPM has proven to be useful in modelling large deformations and dealing with moving boundary conditions, providing more promising results than mesh-based methods.

1.5 THESIS OUTLINE

There are six chapters in total in this report.

1. Introduction
2. Literature review
3. Material Point Method
4. MPM simulation: Verification
5. Wave interaction with porous media
6. Conclusions

Chapter 2: Literature Review

2.1 EXPERIMENTAL AND THEORETICAL INVESTIGATION

2.1.1 Frictional dissipation of wave energy

One of the first investigations into frictional dissipation of wave energy by a porous media was conducted by Savage and Fairchild in 1953 (20). The study of the energy loss by bottom friction and percolation was carried by using a wave flume with a splitter (20). It is found that the maximum energy loss was about 60% under the condition of artificial ripples and permeable bottom of sand (20). In addition, the maximum loss of friction agreed with the theoretical values (20). For the sand grain sizes that are larger than 2 mm, the large amount of percolation losses was detected compared to that for low permeable sands (20). This implies that the porous media is effective in dissipating wave energy, but the amount of energy dissipated is dependent on the porosity of the material used (20).

2.1.2 Wave interaction with porous media

Staub et al. (1957) were one of the first to study wave interactions with a porous media (41). The investigation found that a material with a high porosity was more desirable (41). Additionally, crushed rocks having a high enough porosity were almost as effective as metal meshes on low surface slopes (41). Lean (1967) studied the wave reflection from simple permeable wave absorbers and found that some reflection will always occur (8).

Sulisz (1985) devised a theory predicting wave reflection and transmission at an infinite rubble-mound breakwater when the incident wave meets the structure from a normal direction which showed a reasonable agreement with experimental results (42).

Liu et al. (1999) investigated a numerical model for wave interaction with porous structures (15). The paper combined the free surface-capturing approach with a novel Cartesian cut cell treatment (15). The Finite Volume Model calculates the two-phase flows outside porous structure based on the Navier-Stokes equations where the model equations describe the flow in the porous structure (15). The numerical model is used to create the breaking wave overtopping a caisson breakwater, which is protected by a layer of armour units (15). The results demonstrate that the porous layer is effective in terms of reducing the overtopping of the caisson breakwater (15).

Sakakiyama and Liu (2001) focused experimentally on wave behaviour and turbulence flows in front of a caisson breakwater, which was covered with wave-absorbing blocks and supported by a rubble mound (38). They concluded that turbulence is generated around the caisson breakwater during a wave breaking process, which significantly affects wave impacts and the scouring process in front of the breakwater (38).

Koraim et al. (2014) investigated the hydrodynamic efficiency of a new type of porous seawall experimentally (23). The observation shows that the run-up and reflection coefficients decrease with increasingly porosity: increasing seawall porosity (n) from n = 0.38 to 0.47 decreases the wave run-up and reflection coefficients by 5-10% (23).

2.1.3 Wave impact

Pressures on coastal structures are generated by breaking waves. A wave breaking directly onto a wall will produce much greater impact pressures than a non-breaking wave. Thus, impact pressures are highly relevant to the design of coastal flood defences.

Hattori et al. (1994) performed experiments for wave impact on vertical walls under breaking waves (14). It is found that when a small bubble of air is trapped between a breaking wave and the wall at collision, the impact pressure increases considerably (14). This leads to that the highest impact pressure occurs when the smallest air bubble is trapped between the wall and the wave face (14).

Bullock et al. (2007) carried out a detailed investigation into the characteristic of wave impacts against both vertical and inclined wall (2). They found that the most substantial impact pressures occur at the still water level (2). They also observed that nominally identical waves may produce very different pressure distributions, but similar impulses- the impulse on a structure during impact is shown to be broadly proportional to the peak momentum flux of the incident waves (2).

2.1.4 Vegetation

Vegetation is considered to be one of many shore protection solutions. In addition, there is evidence showing that an area with vegetation could be impacted less from water waves such as tsunami when compared to one without vegetation. This is could be seen from the coastal area in the aftermath of the Indian Ocean tsunami which is shown in Figure 2.1. Therefore, there is an increasing interest in using vegetation along the coast to control wave energy (12).

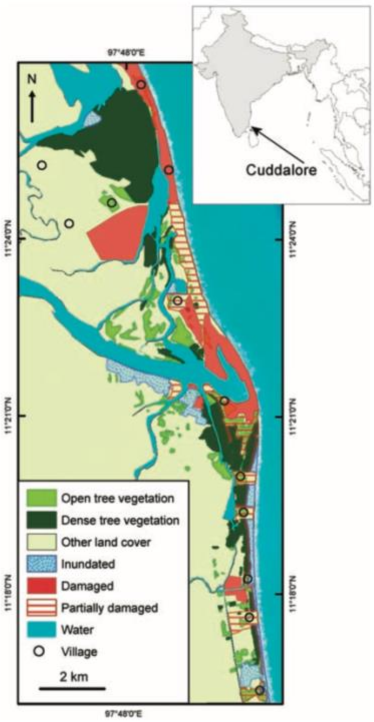

Figure 2.1 – Pre-tsunami vegetation cover and post-tsunami damages in Cuddalore District, India (9)

2.1.5 Summary

The understanding of wave motion and impact has significantly improved over a few decades due to advancements in measurement precision. However, only a few analytical models have been developed and validated while many physical experiments have been conducted. The major difficulties with laboratory experiments outlines above include scaling effects and also flexibility of planning and use.

Recent research has tended to use laboratory experiments to investigate basic physical problems such as the simple dam-breaking and solitary wave propagation scenarios. These results can be used to validate simulations and numerical models, which can then be used to carry out more complex investigations.

2.2 PARICLE METHODS

2.2.1 Smoothed Particle Hydrodynamics (SPH)

The smoothed particle hydrodynamics (SPH) method is a fully Langrangian particle method, in which a continuum material is divided into a set of particles with constant mass, and each particle is assigned a spatial distance (called a smoothing length) in which the physical properties of each particle is smoothed using a kenel function. SPH is widely used in hydrodynamics research. Therefore, the use of SPH to model wave interaction with offshore structures is an active research area in hydrodynamics and coastal engineering. In addition, it has been widely used in the field of wave propagation and wave-structure interaction (27). Although SPH is widely applied in research, it has certain disadvantages for geotechnical problems, many of which involve boundary interfaces (soil-structure interaction). The accuracy of SPH near the boundaries is reduced since there are insufficient neighbouring particles, resulting in a loss of consistency.

The mesh-free SPH method is well suited to handle problems with the large free surface deformations such as wave breaking and wave impacting that arise during the dam break flows problem considered in this project, when compared to a Eulerian approach (27). However, difficulties arise when handling boundary conditions due to the lack of background mesh, which creates complexity in computation when taking the porous nature of the structures into consideration. The SPH approach is more challenging for the geotechnical problem of fluid-structure interaction due to the boundary interfaces. In order to reproduce the behaviour of the fluid flow within the porous medium, an extremely high resolution of SPH particles would be necessary, resulting in prohibitively high computational costs (45). The SPH method was therefore considered less suitable than the material point method for the purposes of this project. 1

2.2.2 Material Point Method (MPM)

This study adopts the material point method (MPM) whereby Lagrangian point masses (called material points) are moved through a Eulerian background mesh. Although there is a mesh, it is used only to solve for the governing equations for computational convenience. In addition, the mesh does not carry permanent information. The key benefit of MPM is that the application of boundary conditions is straightforward due to the presence of background grid. This is because the boundary conditions can be directly applied to grid nodes which is identical to the Finite Element Method (FEM) (4). The formulation is dynamic and includes a no-slip contact algorithm automatically which make MPM helpful for solving problems in which involve large deformations and displacements, velocities and accelerations (33).

MPM has had a key impact in engineering fields in terms of its ability to simulate large deformations without the limitation of mesh tangling. The single-phase MPM has been utilised in various geotechnical problems that involve large deformations, for example, modelling anchors in soils (5), where the soil is considered as a single-phase material. More recently, MPM has been extended to solve multi-phase problems in saturated porous media (1) and unsaturated porous media (46). The interaction between two phases has been formulated in two different manners, either adopting one set of material points (19) or two sets (1) (multiple-point formulation).

Sulsky et al. (1995) was the first to extend MPM to solid mechanics (44). Since then MPM has been widely applied to water-soil interaction problems. Martinelli and Rohe (2015) modelled the fluidization and sedimentation process in MPM, including the simulation of the transition from water to ground water (29).

Zhao and Liang (2016) modelled a seepage flow through embankment using MPM with two sets of material points, representing soil and fluid separately (47). Zhao and Liang (2017) simulated collapsing water columns with different initial aspect ratios via MPM (48). To identify the accuracy and stability of MPM, the simulations are first validated using experimental data and results of other numerical models (48). MPM then produced the reasonable results for the pressure distribution and propagation of dam-break flow (48).

This two-point formulation allows modelling of coupled soil-water behaviour such as changes in the location of the phreatic surface with time, by computing the movements of the fluid particles within the soil. This initial formulation assumed only a small deformation of soil; the same interpolation function was used for both the solid and the fluid layers (27).

Subsequent work has been carried out to develop the MPM code further to allow for more precise modelling of partially saturated soil. However, the interest of this project is the effect of changing the porosity, grain size and height of a carrier on the interaction with a water wave, so complex models of partially saturated soils are currently only of limited interest.

2.2.3 Summary

MPM has been proven to be useful in modelling large deformations and dealing with moving boundary conditions. This project investigates the wave interaction with a porous media, and the soil-water interaction therefore must be considered.

This project involves boundary interfaces as many geotechnical problems and in using SPH, the accuracy near the boundaries is decreased, due to having insufficient neighbouring particles. The single-phase MPM has already been utilised in various geotechnical problems involving large deformations. Furthermore, the two-phase MPM is more widely researched than the two-phase SPH. This project has therefore chosen MPM as the most suitable method for studying the water-wave interaction with a porous media.

Chapter 3: Material Point Method

3.1 MATERIAL POINT METHOD (MPM)

The material point method (MPM) uses a continuum based on soil constitutive models, for example the Mohr-Coulomb, Cam Clay or Modified Cam Clay models. Instead of grains, the material points (MPs) are viewed as representative volume elements (RVE). In MPM, the computational domain is spatially discretised in two frames, as shown in Figure 3.1. Firstly, the continuum body is divided into a group of MPs. Each particle carries all the material variables: mass, velocity, stress, strain and position, which makes the MPM convenient for modelling based on history-dependent constitutive material points. Each point also has a constant mass but has a volume which can change. This enables compression or extension of material and then each MP moves with the body deformation. The mass and constitutive equations are solved at the MPs.

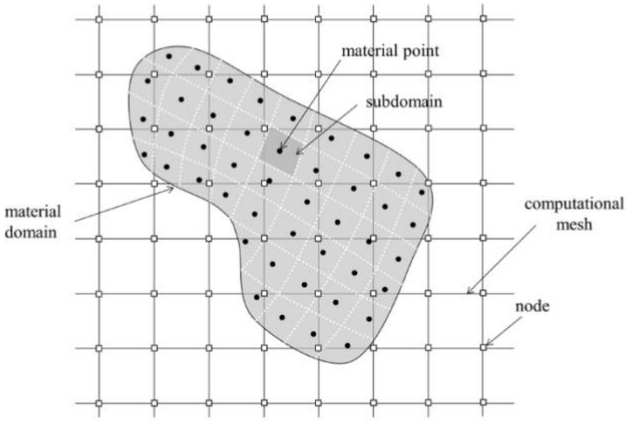

Figure 3.1 - Space discretisation of a continuum body showing nodes of the computational mesh and material points (37)

The computational mesh is equivalent to a conventional finite element mesh and covers the full domain of the problem, including empty spaces in which particles may have to move into. The momentum equations are solved at the nodes of this computational mesh. The variables required to solve the governing equations for each step of the calculation are transferred from the material points to the nodes of the mesh via mapping functions. Boundary conditions are imposed, either at the mesh nodes or at the MPs, and an incremental scheme is used to solve the governing equations. The quantities carried by the MPs are updated through the interpolation of the mesh results, via the same mapping functions. In addition, the information associated with the mesh can be discarded to avoid any mesh distortion, as it is not needed for the next step of the analysis.

In MPM, as it is the particle and is not the mesh points that store all the information on the state of the calculation, no numerical error results from the mesh returning to its original position after each step and no re-meshing is required. Once the momentum balance equation is solved at each node of the background mesh and the location of the MPs has been updated the background mesh is reset to the original position as shown in Figure 3.2 below.

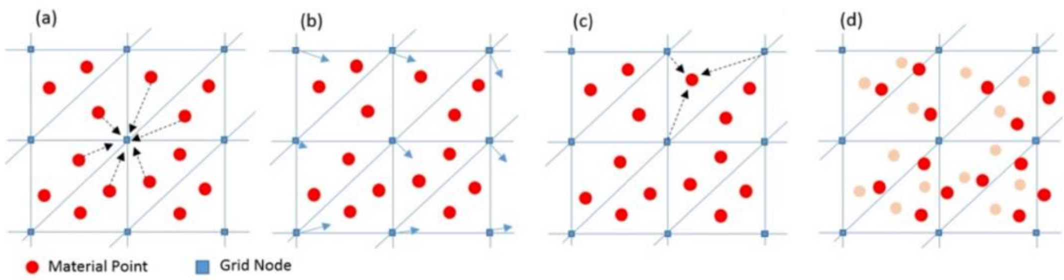

Figure 3.2 - Computation scheme of MPM: (a) map information from MPs to grid nodes; (b) solve governing equations of motion at the nodes; (c) update MP information; (c) update MP position and housekeeping (41)

Following MPs is difficult to implement in a Eulerian scheme. Meanwhile, modelling using just Langragian methods is likely to cause severe mesh distortion, leading to mesh lock-up or entanglement. In MPM, mesh tangling is avoided since the fixed Eulerian grid can be interpolated as an updated Lagragian frame of reference and so the usual convection term in acceleration associated with Eulerain formulations does not appear (43).

MPM has proven to be useful in modelling large deformations and dealing with moving boundary conditions. Additionally, it has several advantages over the smoothed particle hydrodynamics (SPH) method, where a continuum material is divided into a set of particles. There is a parameter called a smoothing length which each particle is assigned a spatial distance and the physical properties of each particles is smoothed using a kernel function. SPH encounters problems involving boundary interfaces (such as the soil-water interface), particularly a reduction in accuracy near boundaries since insufficient neighbouring particles result in a loss of consistency. Since two-phase MPM is more widely researched than two-phase SPH and the fact that the soil-water interaction is critical in this project, MPM has been chosen as the most suitable method for studying water-wave interaction with porous media.

3.2 GOVERNING EQUATIONS

The understanding of dam-break flow theory is provided by the shallow water theory. Discontinuities in the weak form of the solution can be used to represent shocks in the flow due to the shallow water equations (SWEs).

To obtain the SWEs, the three-dimensional Navier-Stokes equations need to be integrated. Even though the formulation of the SWEs is not investigated in this project, these equations are often favoured in flood simulations with the convenient and accurate description for almost horizontal flows (47).

The material domain Ω is represented by a number of material points N_p and the position of the material point at the current instant (time t) is denoted by x_p. The same material point at the initial time ($t\ = 0$) is denoted x_p^0. The governing equations describing the continuum body are the standard conservation equations: mass (Equation 3.1) and momentum (Equation 3.2).

$$\frac{\partial \rho}{\partial t} + \rho \Delta \cdot \nu = 0 \qquad (3.1)$$

$$\rho \mathbf{a}\ =\ \Delta \cdot \sigma =\ \rho \mathbf{b} \qquad (3.2)$$

where $\rho(x,t)$ is the density of the continuum body, acceleration $\boldsymbol{a}(x,t)$ is the material derivative of the velocity $v(x,t)$, $\boldsymbol{b}$ is a specific body force and σ is the Cauchy stress tensor that can be decomposed into pressure and deviatoric components.

The water pressure is linked to its density change:

$$p = p_0 + K\frac{\rho}{\rho_0} \qquad (3.3)$$

where K is the bulk modulus of water, p is pressure, and the subscript indicates an initial reference value.

In the MPM, the Langrangian framework removes the need for a non-linear convective term. The positions of each material point are updated with every timestep.

3.3 WEAK FORM OF THE GOVERNING EQUATIONS

Each material point carries the field variables, mass M_p, density $\rho(x,t)$, velocity $v_p(x,t)$ and the Cauchy stress $\sigma(x,t)$, for $p = 1,2,3, \ldots N_p$. Since the mass M_p is constant throughout the computation, the mass is automatically conserved in MPM.

At the current instant, the density of the continuum body can be expressed as:

$$\rho(\boldsymbol{x}, t) = \sum_{p=1}^{N_p} M_p \, \delta(\boldsymbol{x} - \boldsymbol{x_p}) \qquad (3.4)$$

where δ( ) is the Dirac delta function.

This leads to the following relationship:

$$\int \rho dV = \sum M_p \delta(\boldsymbol{x} - \boldsymbol{x}_p) dV \qquad (3.5)$$

The weak form of the momentum equation can then be formed by multiplying the equation of conservation of momentum by a test function w:

$$\int_{\Omega} (\rho \boldsymbol{w} - \boldsymbol{w} \Delta \cdot \sigma - \rho \boldsymbol{w} \cdot \boldsymbol{b}) dV = 0 \qquad (3.6)$$

Applying the divergence theorem to Equation 3.6 allows us to write the weak form of the momentum equations as:

$$\int_{\Omega} \rho \boldsymbol{w} \cdot \boldsymbol{a} dV = -\int_{\Omega} \sigma : \Delta \boldsymbol{w} dV + \int_{\Omega} \rho \boldsymbol{w} \cdot \boldsymbol{b} dv + \int_{\partial\Omega} \boldsymbol{w} \cdot \tau dS \qquad (3.7)$$

Let $M_p = \int \rho dV$, we can approximate Equation (3.7) by a summation of quantities at material points:

$$\sum_{p=1}^{N_p} M_p \boldsymbol{w}(\boldsymbol{x_p}, t) \cdot \boldsymbol{a}(\boldsymbol{x_p}, t) = -\sum_{p=1}^{N_p} M_p \, \sigma^s(\boldsymbol{x_p}, t) \colon \boldsymbol{w}(\boldsymbol{x}, t)|_{x=x_p}$$
$$+\sum_{p=1}^{N_p} M_p \, \boldsymbol{w}(\boldsymbol{x_p}, t) \cdot \boldsymbol{b}(\boldsymbol{x_p}, t) \qquad (3.8)$$
$$-\int_{\partial\Omega} \boldsymbol{w} \cdot \boldsymbol{\tau dS}$$

where σ^s is a specific stress.

3.4 DISCRETISATION

If a Eulerian grid with a total number of nodes N_n is considered, standard nodal basis foundations, $N_i(x)$ with $i = 1 - N_n$ can be defined in the same way as in standard Finite Element Method (FEM). Rewriting the acceleration $\boldsymbol{a}(x, t)$ and test function $\boldsymbol{w}(x_p, t)$ at material points x_p in terms of nodal basis functions gives the following equations:

$$\boldsymbol{a} = \sum_{i=1}^{N_n} \boldsymbol{a}_i(t) N_i(\boldsymbol{x}) \qquad (3.9)$$

$$\boldsymbol{w} = \sum_{i=1}^{N_n} \boldsymbol{w}_i(t) N_i(\boldsymbol{x}) \qquad (3.10)$$

We can substitute these to Equation 3.7, resulting in a discretised equation below (4.3):

$$\sum_{i=1}^{N_n} \boldsymbol{w_i} \cdot \sum_{j=1}^{N_n} \boldsymbol{m_{ij}}\, \boldsymbol{a_j} =$$

$$-\sum_{i=1}^{N_n} \boldsymbol{w_i} \cdot \sum_{p=1}^{N_p} \boldsymbol{M_p}\, \boldsymbol{\sigma_p^s} \cdot \boldsymbol{\Delta N_i}(x)|_{x=x_p} + \sum_{i=1}^{N_n} \boldsymbol{w_i} \cdot \boldsymbol{b_i} + \sum_{i=1}^{N_n} \boldsymbol{w_i} \cdot \boldsymbol{\tau_i} \qquad (\mathbf{3.11})$$

where the mass matrix, m_{ij}, defined as:

$$m_{ij} = \sum_{p=1}^{N_n} M_p N_i(\boldsymbol{x_p}) N_j(\boldsymbol{x_p}) \qquad (3.12)$$

The applied traction, τ_i, is:

$$\tau_i = \int_{\partial\Omega} \tau(\boldsymbol{x}, t) N_i(\boldsymbol{x}) dS \qquad (3.13)$$

And the specific body force, $\boldsymbol{b}_i$, is:

$$\boldsymbol{b_i} = \sum_{p=1}^{N_n} (\boldsymbol{x}, t) N_i(\boldsymbol{x}_p) \qquad (3.14)$$

Then, considering the arbitrary nature of $\boldsymbol{w}_i$, we can rewrite Equation (3.11) in a reduced form. From this, we can solve for the acceleration $\boldsymbol{a}$ at the grid nodes by solving $\boldsymbol{N}_n$ coupled linear equations.

$$\sum_{\mathrm{j=1}}^{\mathrm{N_n}} m_{ij} \boldsymbol{a}_j = \boldsymbol{f}_i^{int} + \boldsymbol{f}_i^{ext} \qquad (3.15)$$

where $\boldsymbol{f}_i^{int} = -\sum_{p=1}^{N_p} M_p\, \Delta N_i(\boldsymbol{x})|_{x=x_p} \cdot \sigma_p^s$

$$\boldsymbol{f}_i^{ext} = \boldsymbol{b}_i + \tau_i$$

3.5 TWO-PHASE FORMULATION

MPM can deal with soil and liquid simultaneously. To allow for this, the solid and liquid phases are assigned separate sets of material points, such that saturated soil can be regarded as soil particles floating within a fluid or a porous medium surrounded by liquid. The momentum balance equations for the MP layers are presented by separate velocity fields as follows:

$$\nabla \cdot \sigma_s' + n_s \nabla \cdot \sigma_l + \bar{\rho}_s \boldsymbol{g} + \boldsymbol{f}_d = \bar{\rho}_s \frac{du_s}{dt} \qquad (3.16)$$

$$n_l \nabla \cdot \sigma_l + \bar{\rho}_l \boldsymbol{g} - \boldsymbol{f}_d = \bar{\rho}_s \frac{du_l}{dt} \qquad (3.17)$$

where the subscripts s and l denote the solid and liquid respectively, $\bar{\rho}$ is the partial density, n is the concentration ratio defined as the ratio of the partial density $\bar{\rho}$ to the corresponding mass density and $\boldsymbol{f}_d$ is the drag force by the liquid on the soil. It is calculated from the Darcy equation as follows:

$$\boldsymbol{f}_d = n_L^2 \frac{\mu}{\kappa} (\boldsymbol{u}_l - \boldsymbol{u}_s) \qquad (3.19)$$

where κ is the intrinsic soil permeability. The Kozeny-Carmen formula below is used to evaluate the soil permeability.

$$\kappa = \frac{D^2}{A} \frac{n^3}{1 - n^2} (3.20)$$

where D is the effective grain size diameter (m), n is the soil porosity and A is a constant, equal to 150 (10).

When two sets of material points are used, the mixture must be identified by its state, characterised by the dominant material. To determine which state is appropriate, an additional parameter n_{max} is represented the maximum porosity. A mixture with an initially solid state that undergoes fluidisation is characterised by two aspects: the mean effective stress decreases and the porosity increases. The mean effective stress may become zero when there are no longer contact forces between the grains. Fluidisation only occurs if the grains are significantly separated, so that the porosity is larger than n_{max} and the state becomes liquid. In the reverse process, sedimentation, the porosity decreases as the solid grains become closer to each other. However, the effective stresses arise only if the porosity is smaller than n_{max} (i.e. the grains are close enough to be in contact) and the state is solid.

3.6 NUMERICAL IMPLEMENTATION

During the course of the MPM computation, the unknown variables are always recorded by the material points and interpolated onto the grid at the beginning of each time step. In order to eliminate divisions by nodal masses, momentum is used in place of velocity as much as possible in the code. Further, the velocity gradient used to calculate the strain rate at material points is calculated using the updated particle velocities mapped onto the grid nodes (44).

The general computation procedure in each time step is as follows:

1. Initialise the grid and material points.
2. Extrapolate material point quantities to grid nodes
3. Solve equations of motion on the grid
4. Solve Equation 3.15 to obtain the nodal acceleration
5. Extrapolate derivative terms back to the material points
6. Grid is reset and material point positions is updated.

Chapter 4: MPM simulation: Verification

4.1 LIQUID DAM-BREAK FLOWS

The basis of the investigation is water-wave impact on porous medias with the MPM model, which is therefore validated through a comparison of a liquid dam-break flow against existing numerical and experimental data.

Viscous and turbulent effects are not considered in dam-break floods. In addition, all surfaces are assumed to be frictionless.

4.1.1 Definition of geometry and mesh

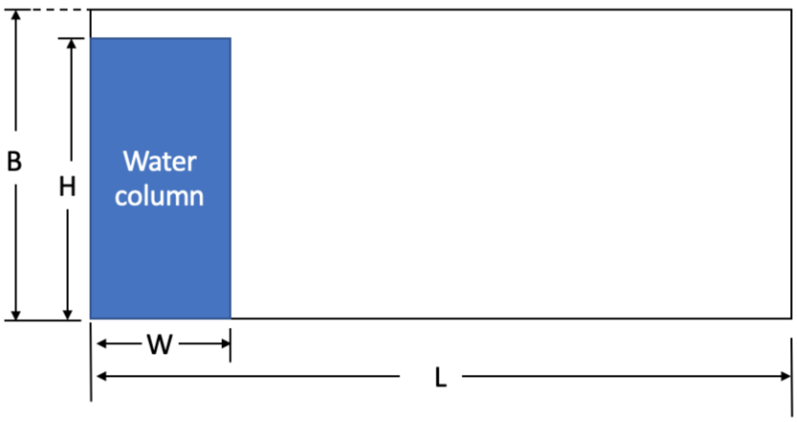

Figure 4.1 – Initial geometry of liquid dam-break simulation

The initial geometry is shown in Figure 4.1 above.

4.1.2 Boundary conditions

In this simulation, the right, left, top and bottom surfaces of the flume are fixed to prevent movement of material points outside the computational domain.

4.1.3 Parameters

To ensure consistency in simulation resolution, the number of material points (MPs) and the size of the domain was altered. Due to the investigation in Zhao et al. (2017), it is found that the mesh size and particles density do not play an important role in the results of dam-break simulations.

Table 4.1 – Dam-break simulation parameters

Ratio α	**Height H(m)**	**Width W(m)**	**Depth D(m)**	**Box height B(m)**	**Box width L(m)**	**Mesh size (m)**	**MPs**
2	2	1	0.1	2.2	5	0.1	8

4.1.4 Material properties

The material properties for the liquid dam-break simulation are shown in Table 4.2. To achieve a relatively large time step, an unrealistically low bulk modulus of waster was chosen, as in Zhao et al. (2017). This results in increased compressibility and it does not affect the simulation if the speed of the modelled water is over ten times larger than the maximum flow speed across the domain.

Table 4.2- Material properties of the dam-break simulation

Material	**Water**
Material type	Liquid
Bulk modulus (kPa)	20,000
Dynamic viscosity (kPa/s)	1e-6
Density ρ(kg/m^3)	1,000
Liquid cavitation (kPa)	0
Detect free surface	Yes

4.1.5 Results

4.1.5.1 Validation

The results from liquid dam-break flow are compared with the validated results in Liang (2010), where the column collapse is modelled using SPH. These results are shown in Figure 4.3. The MPM code illustrates excellent agreement in both the shaped and the pore pressure.

4.1.5.2 Parameters

To compare the results, distance and time have been scaled according to the Froude law:

$$t^* = \frac{t}{\sqrt{H/g}} \qquad (4.1)$$

$$x^* = \frac{x}{H} \qquad (4.2)$$

where t^* is the normalized time, $x^*$is the normalized position of the flood front, t is time, x is the position of the flood front, H is the initial height of the water column and x is the gravitational acceleration.

A quantitative comparison of the position of the flood front in the MPM simulations is compared to published results for SPH, Volume-of-Fluid (VOF) and shallow water equations (SWEs) and the experimental data is shown in Figure 4.2. The flow front position is defined as the position of the most front particle with a continuous stream of particles following and any small dispersed particles leading to the flow are ignored. However, there is potential for errors since front positions are obtained by visual identification.

The MPM simulations seem to agree well with previously verified MPM simulations, both the experimental data and the previously published numerical results. The SWEs solver overestimates the propagation speed. This is because of negligible vertical momentum and is therefore not considered in this analysis.

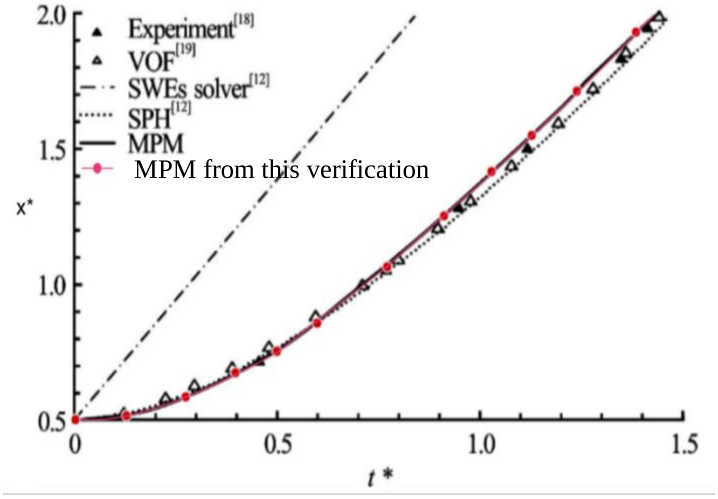

Figure 4.2 - Change in flood front position with time (Compared with the published results from Zhao et al. (2017))

Time (s)	SPH (Liang, 2010)	MPM
0	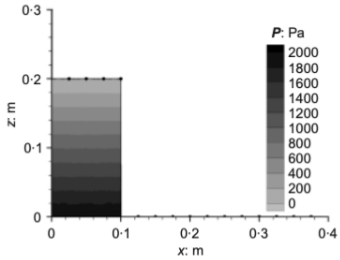	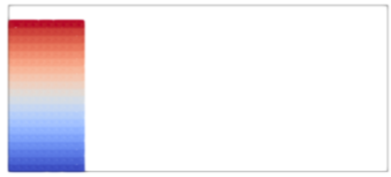
0.03	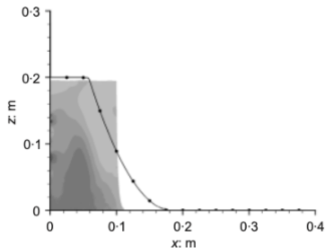	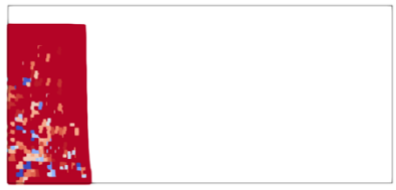
0.07	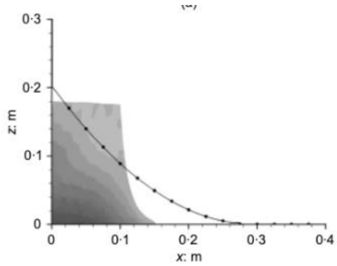	
0.10	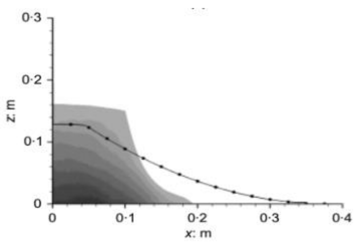	
0.15	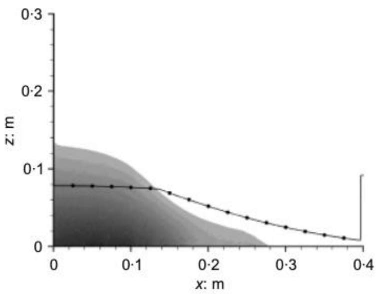	

Figure 4.3 - Comparison of the results produce by Liang in SPH with the results produced by MPM on the right.

4.2 POROUS SEAWALL

The solid-wall simulations capturing dam-break flow formed the basis for numerically investigating the impact of this type of wave of porous media. The ability of the MPM code to produce reliable results for wave impact on porous media was verified by extensive comparison of simulation results with numerical and experimental results published in Liu et al. (1999).

4.2.1 Definition of geometry and mesh

The initial geometry is shown in Figure 4.4. The experiments conducted by Liu et al. (1999) used a water tank of $0.892\ \mathrm{m} \times 0.44\ \mathrm{m} \times 0.55\mathrm{m}$. A porous structure of $0.29\ \mathrm{m} \times 0.44\ \mathrm{m} \times 0.37\ \mathrm{m}$ was built with crushed rocks ($D_{50} = 1.59\ \mathrm{cm},\ n = 0.49$) was placed at the centre of the tank, from $x = 0.3 - 0.59\ \mathrm{m}$. A gate was constructed $2\ \mathrm{cm}$ away from the porous structure and pulled up manually within $0.1\ \mathrm{s}$ at the beginning of the test. The initial water level was $0.25\ \mathrm{m}$. The numerical set-up is the same as the experimental set-up except that there is a gap of $2\ \mathrm{cm}$ between the water column and the near side of the porous dam.

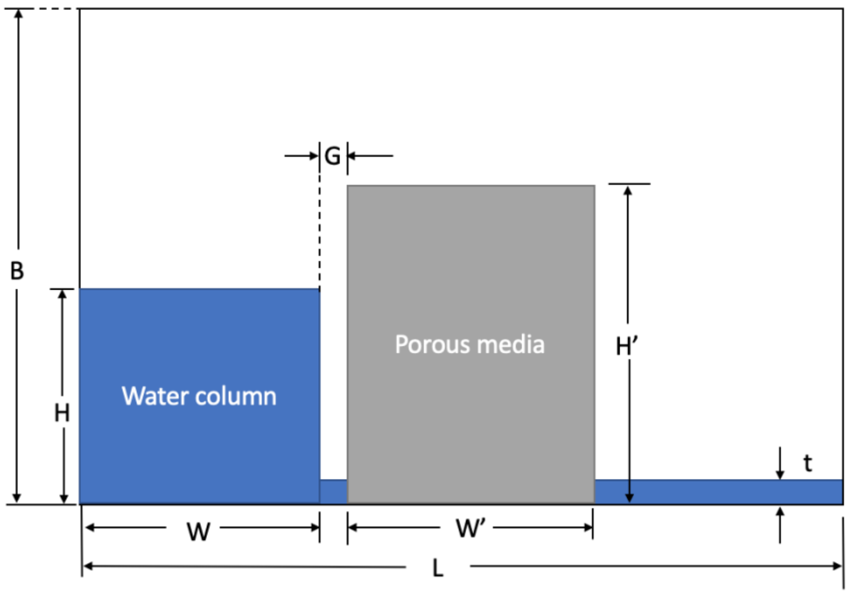

Figure 4.4 – Initial geometry of porous wall simulation

4.2.2 Boundary conditions

In this simulation, the right, left, top and bottom surfaces of the flume are fixed to prevent movement of liquid material points outside the computational domain. In addition, the boundary of the porous media shown in Figure 4.4 is fixed to prevent movement of solid material points outside the media in all the surfaces.

4.2.3 Parameters

Table 4.3- Porous wall simulation parameters

Height H(m)	**Width W(m)**	**Depth D(m)**	**Box height B(m)**	**Box width L(m)**	**Height H'(m)**	**Width W'(m)**	**Gap G (m)**	**Thickness t(m)**
0.25	0.28	0.44	0.58	0.892	0.37	0.29	0.02	0.025

4.2.4 Material properties

The material properties for the porous wall simulation are shown in the Table 4.4 below:

Table 4.4 -Material properties in porous wall simulation

Material	**Water**	**Dry crushed rocks**	**Saturated crushed rocks**
Material type	Liquid	Dry Material	Saturated material-fully coupled
Initial porosity	-	0.49	0.49
Density solid(kg/m^3)	-	2,650	2,650
Density liquid (kg/m^3)	1,000	-	1,000
Intrinsic permeability liquid (m^2)	-	-	7.623e-7
Bulk modulus (kPa)	20,000	-	20,000
Dynamic viscosity (kPa/s)	1e-6	-	1e-6
Material model	-	Linear Elasticity	Linear Elasticity
Effective Poisson ratio	-	0.3	0.3
Effective Young modulus	-	10,000	10,000

In the double-point MPM code, permeability is related to the interaction force vector between the liquid and the soil particles, resulting from the drag force exerted on the solid particles by the fluid.

The permeability of the porous block is described by the Kozeny-Carmen equation:

$$\kappa = \frac{D^2}{A}\frac{n^3}{1-n^2} \qquad (4.3)$$

where κ is the permeability (m^2), D is the effective grain size diameter (m), n is the soil porosity and A is a constant, equal to 150 (Ergun, 1952).

The initial geometry and permeability parameter are matched to the experiments in Liu (1999) as shown below:

$$\kappa = \frac{0.0159^2}{150}\frac{0.49^3}{1-0.49^2}$$

$$\therefore \kappa = 7.623 \times 10^{-7} m^2$$

4.2.5 Results

Figure 4.5 illustrates the comparisons of free surface profiles for the flow passing through the porous dam at different points, compared with the numerical and experimental results from Liu et al. (1999). It demonstrates that after the gate is open, or the simulation is started, the water column immediately begins to collapse and fluid particles rush towards the porous media. After $\boldsymbol{t = 0.20\ s}$, water particles have filled the gap between the initial water column and the porous dam, and a dam-break flow begins to develop. Since the porous dam offers some resistance to the flow, the particles stack up and rise to form a small upward jet which then develops inside the leading edge of the dam at $\boldsymbol{t = 0.40\ s}$. This jet can be observed in both the numerical and experimental results. Some of the impacting water is reflected by the porous boundary to form a wave traveling back towards the left side of the tank which reaches the wall before being totally re-reflected by the solid boundary back towards the dam. The free fluid domain on the left side of the tank shows a free surface oscillation driven by the gap between the initial water column and the porous dam. The frequency of this oscillation is comparable to the natural frequency of the water body contained on the left side of the tank which is similar to harbour oscillations. This fluctuation gradually decreases as particles pass through the porous dam. Meanwhile, water particles escape from the far boundary of the porous dam and propagate towards the right tank boundary which arrive at the wall at $\boldsymbol{t = 1.0\ s}$ and reflects back again to form a similar oscillation on the right side of the media.

The largest discrepancy between numerical and experimental results occurs at $\boldsymbol{t = 0.20\ s}$, where the experimental data indicate a faster advancement of water particles near the bottom inside the porous media. This could be explained by the gate-opening phenomena whereby the manual operation of the gate is non-instantaneous, tanking around $\boldsymbol{0.10\ s}$ and allowing water near the bottom of the tank to be released earlier.

Overall, very consistent agreement between the MPM simulations and the experimental and numerical results published in Liu et al. (1999) is obtained.

Time (s)	Experiment (Liu, 1999)	MPM
0	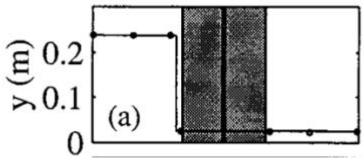	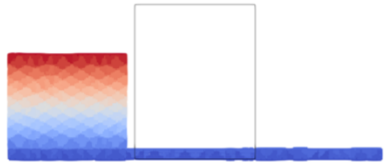
0.4	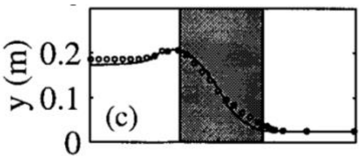	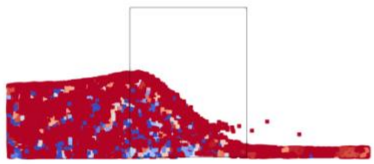
0.8	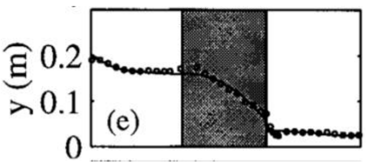	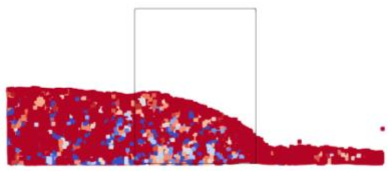
1.2	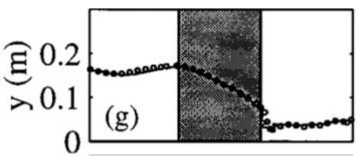	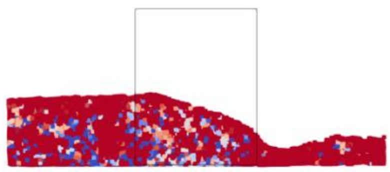
1.6	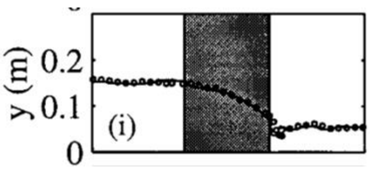	
2.0	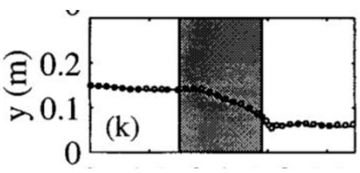	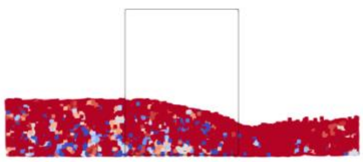

Figure 4.5 - Comparison of the results produce by Liu in experiments with the results produced by MPM on the right.

4.3 CHANGE IN GRAIN SIZE

4.3.1 Material properties

Instead of investigating only 15.9 mm grain size, others are studied which are 1 mm, 5 mm, 10 mm, 50 mm and 100 mm. Other material properties are kept the same as the previous part.

4.3.2 Results

Since the height of the porous column is greater than that of the water column, the overtopping cannot be an issue for this analysis. In addition, water has only one option to travel which is flowing through the porous media. In this specific scenario, the smaller grain sizes are considered to have more impacted on the propagation of water through the media. When the grain sizes between 1 mm and 10 mm are considered, the difference of the water movement is more obvious than when the grain sizes between 50 mm and 100 mm are considered which can be seen in Figure 4.6 on the next page. This could be explained by the fact that the size of the porous barrier is only $0.29\text{ m} \times 0.44\text{ m} \times 0.37\text{ m}$ whose smallest size is only 2.9 bigger than the greatest grain size value which is 100 mm. This calculated value might not be small enough for the porous media containing this grain size.

4.4 CHANGE IN POROSITY

4.4.1 Material properties

Instead of investigated only the porosity value (n) of 0.49, others are studied which are 0.40, 0.60 and 0.90. Other material properties are kept the same as the previous part.

4.4.2 Result

Since the height of the porous column is greater than that of the water column, the overtopping cannot be an issue for this analysis. In addition, water has only one option to travel which is flowing through the porous media. In this specific scenario, water travel through the porous media easier and less violent with the lower value of porosity. In $\mathrm{n} = 0.90$, there is some amount of water particles being pushed upwards and travelling toward the right of flume faster than the bottom part in the porous structure. This can potentially cause damages to anything located behind the barrier. This can be seen in Figure 4.7.

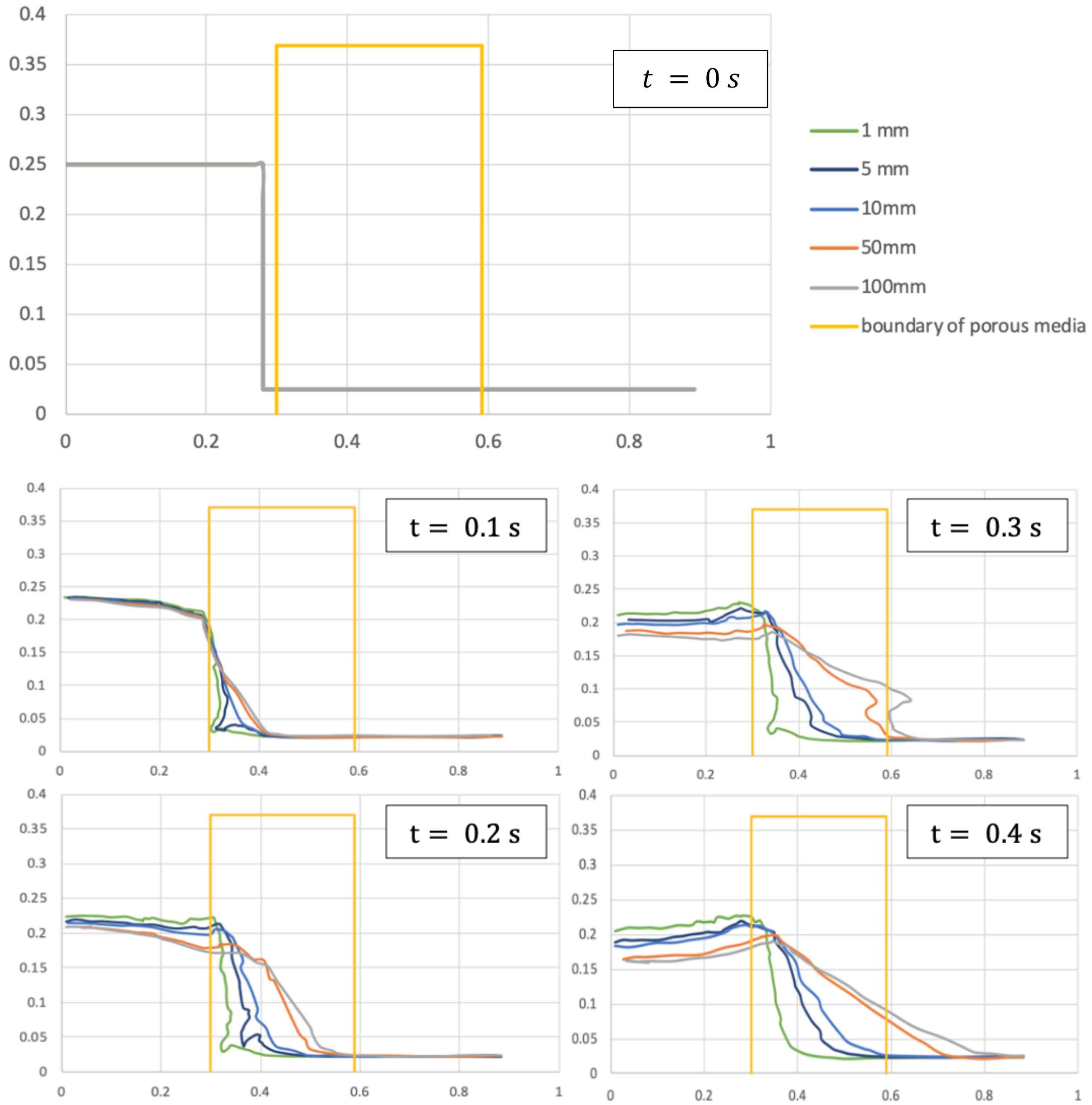

Figure 4.6 – Water propagation through the porous media with different values of grain size

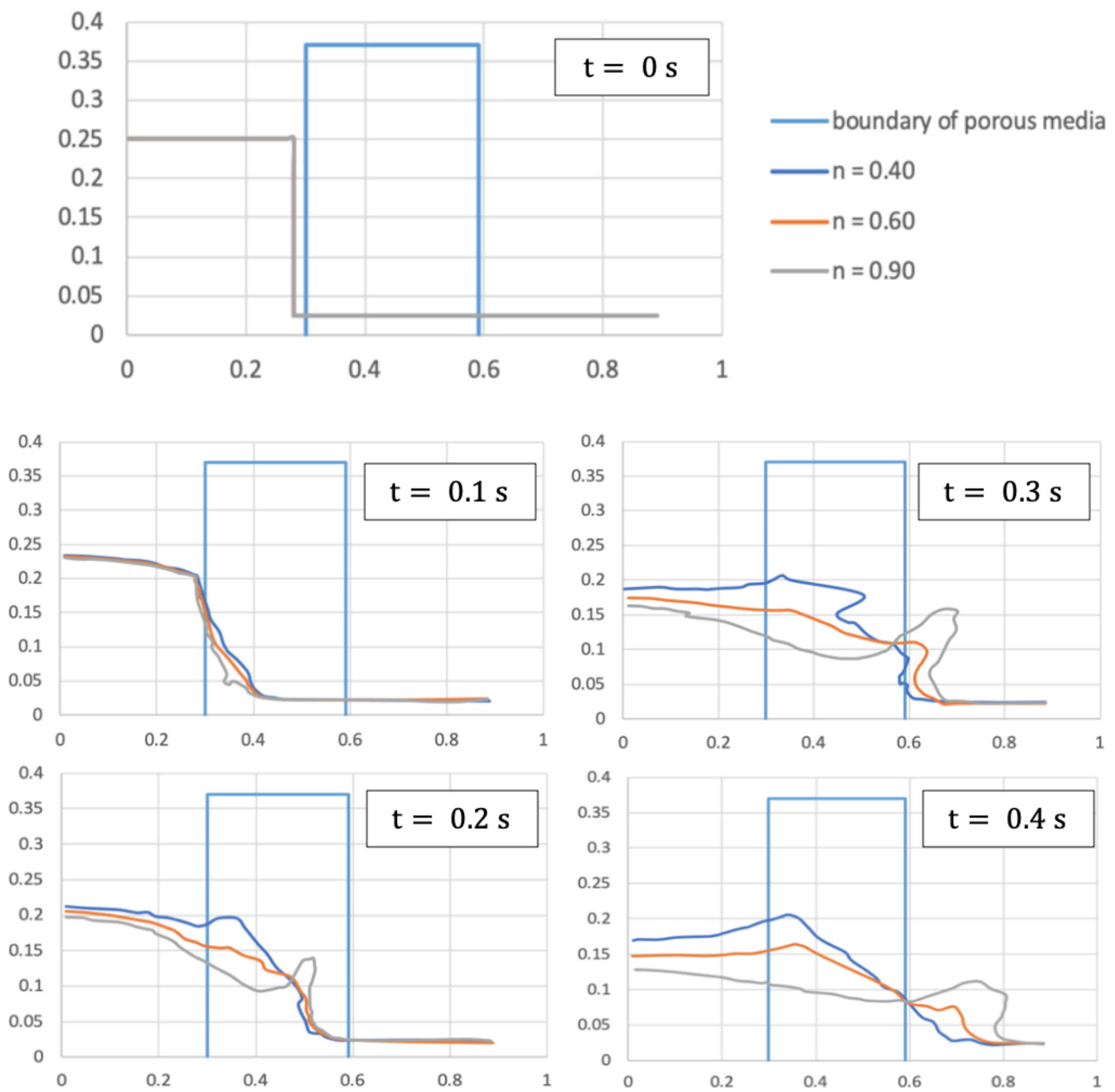

Figure 4.7 – Water propagation through the porous media with different values of porosity

4.5 DISCUSSION

The MPM code has demonstrated results that agree with published results. Compared with other verified numerical simulations and experimental data, the MPM simulations give good predictions of the pressure distribution and the front propagation of dam-break flows. In addition, the movement of water from the change in the porosity in the porous structure and the change in the grain size in the porous structure agrees well with the theory.

From these simulations, it was decided that it was possible to use the MPM to model dam-break flows and to generate a water wave to investigate interaction with a porous medium.

Chapter 5: Wave Interaction with Porous media

5.1 MODEL SETUP

This model setup is used through all of three investigations done in this chapter. However, the height of the porous media (H′) is varied which will be mentioned in each section. This model setup is adapted from the Liu et al. (1999)'s model in the previous section.

5.1.1 Definition of initial geometry

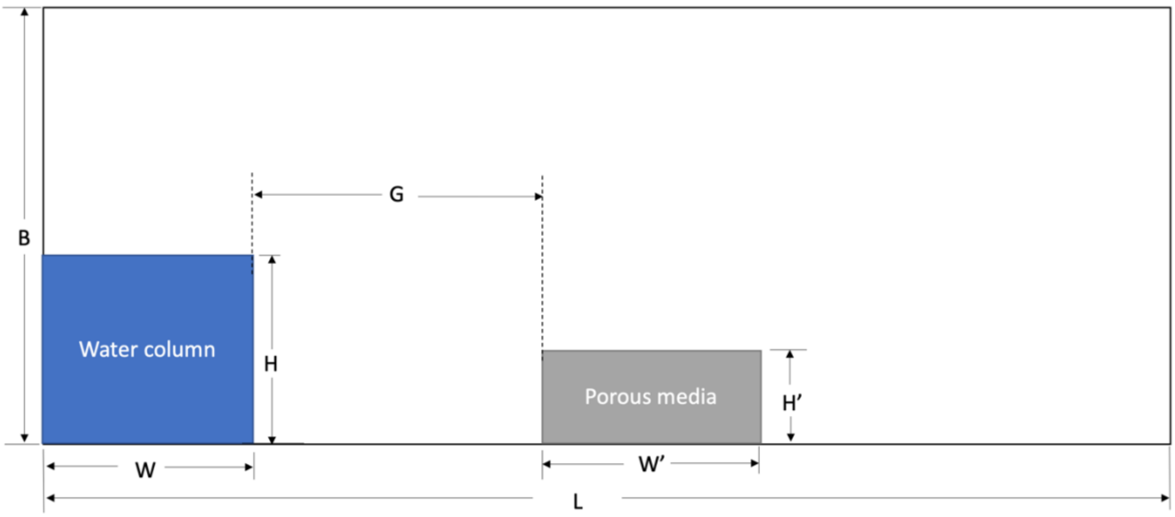

Figure 5.1 – Initial geometry of the investigated simulation

5.1.2 Boundary condition

In this simulation, the right, left, top and bottom surfaces of the flume are fixed to prevent movement of liquid material points outside the computational domain. In addition, the boundary of the porous media shown in Figure 5.1 is fixed to prevent movement of solid material points outside the media in all the surfaces.

5.1.3 Parameters

Table 5.1- Simulation parameters

Height H(m)	**Width W(m)**	**Box height B(m)**	**Box width L(m)**	**Height H'(m)**	**Width W'(m)**	**Gap G (m)**
0.25	0.28	0.58	2.00	varied	0.29	0.72

5.1.4 Material properties

Table 5.2 -Material properties in the investigated simulation

Material	Water	Porous media
Material type	Liquid	Dry Material
Initial porosity	-	0.49
Density solid(kg/m^3)	-	2,650
Density liquid (kg/m^3)	1,000	-
Bulk modulus (kPa)	20,000	-
Dynamic viscosity (kPa/s)	1e-6	-
Material model	-	Linear Elasticity
Effective Poisson ratio	-	0.3
Effective Young modulus	-	10,000

5.2 EFFECT OF HEIGHT ON FRONT FLOOD

5.2.1 Parameters

The heights of the porous media (H') used in this section are 0.05 m, 0.07 m, 0.08 m, 0.10 m and 0.15 m.

5.2.2 Results

From Figure 5.2, it is shown that the speed of water traveling through the porous media is varied and depends on the height of the porous structure. In a higher height of the porous media, the speed of water propagation is lower as illustrated in Figure 5.4. Due to the fact that the same value of grain size is used in all of scenarios, this means that the greater height of the porous media is, the greater number of pores within the porous media is. Therefore, this indicates that water has more space to propagate within the media in the higher porous structure than that in the lower one. The total distance for water to travel in a taller media is greater so it takes more time for water to travel to the other side of the porous media.

In Figure 5.3, there are two cases which are 0.05 m and 0.15 m of the porous media. The differences between those two scenarios can be seen after $\mathrm{t} = 0.35$ s which is when the water wave reached the structure. For $\mathrm{H}' = 0.05$ m, water quickly filled up the pores within the media, which causes the overtopping of the barrier to occur. It can be seen from $\mathrm{t} = 0.40$ s to

$t = 0.60$ s, the amount of water in the overtopping increases and travels to the right of the flume. Meanwhile, for $H' = 0.15$ m, there is no overtopping of the porous media since the water can flow through the media. When the water collides with the porous barrier, some of it is reflected back to the left side of the flume which mean this portion of water is slowed down for travelling to the end of the flume. For the higher structure, the larger portion of water reflected back is slowed down which means that it is more effective to reduce the first portion of water travelling to the end of the flume.

There are two clear trends shown in Figure 5.2. The first trend is similar to the line for the front flood position belongs to the investigation of water column without porous structure (brown line). The first trend has $H' = 0.05$ m and $H' = 0.07$ m. The second trend has $H' = 0.08$ m, $H' = 0.10$ m and $H' = 0.15$ m. Therefore, in the sections 5.3 and 5.4, $H' = 0.07$ m from the first trend and $H' = 0.15$ m from the second trend are selected to represent their groups to investigate the effect of porosity and the effect of grain size to the front flood position.

In Figure 5.4, the greatest difference in speed is between the $H' = 0.05$ m media and the $H' = 0.15$ m media where the two main groups are categorised. It is considered that the change in speed is lower in the latter group. The speed for the simulation without the porous media is approximately 3.05 m/s. The lowest speed is just about 1.45 m/s at $H' = 0.15$ m. The greatest speed is around 2.94 m/s at $H' = 0.05$ m.

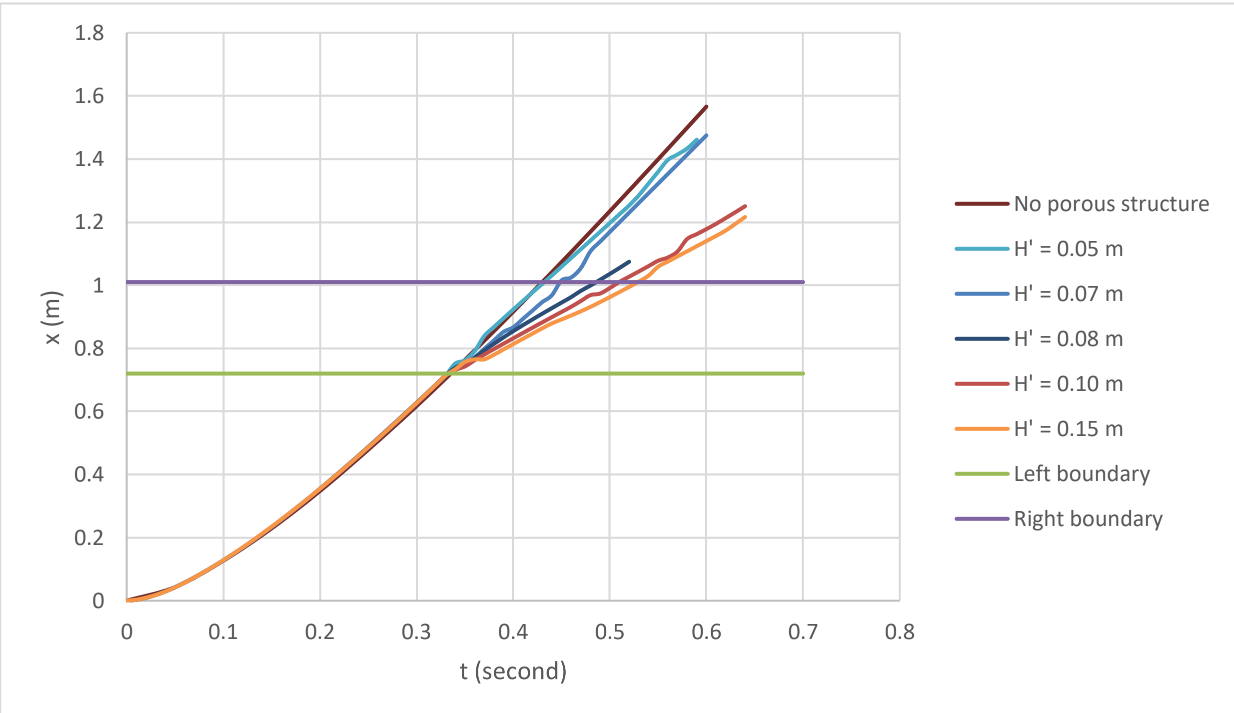

Figure 5.2 – The graph of the front flood position (x) against time for different height values

Time (s)	Height of 0.05 m	Height of 0.15m
0		
0.20		
0.35		
0.40	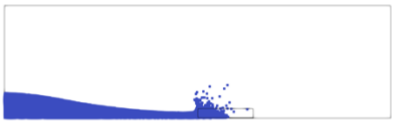	
0.45		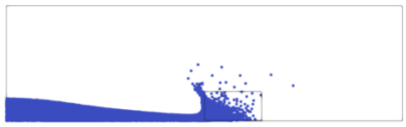
0.50		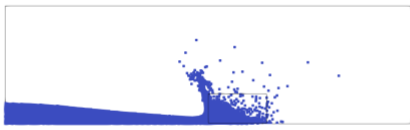
0.55		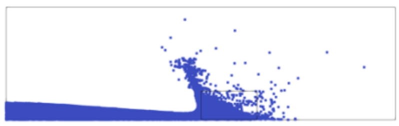
0.60	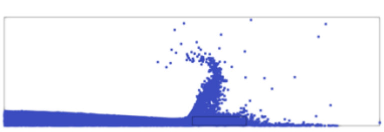	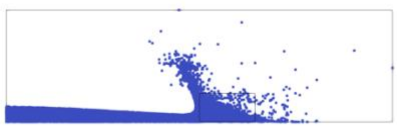

Figure 5.3 - Comparison of the results produce by MPM (on the left height of 0.05 m, on the right height of 0.15m)

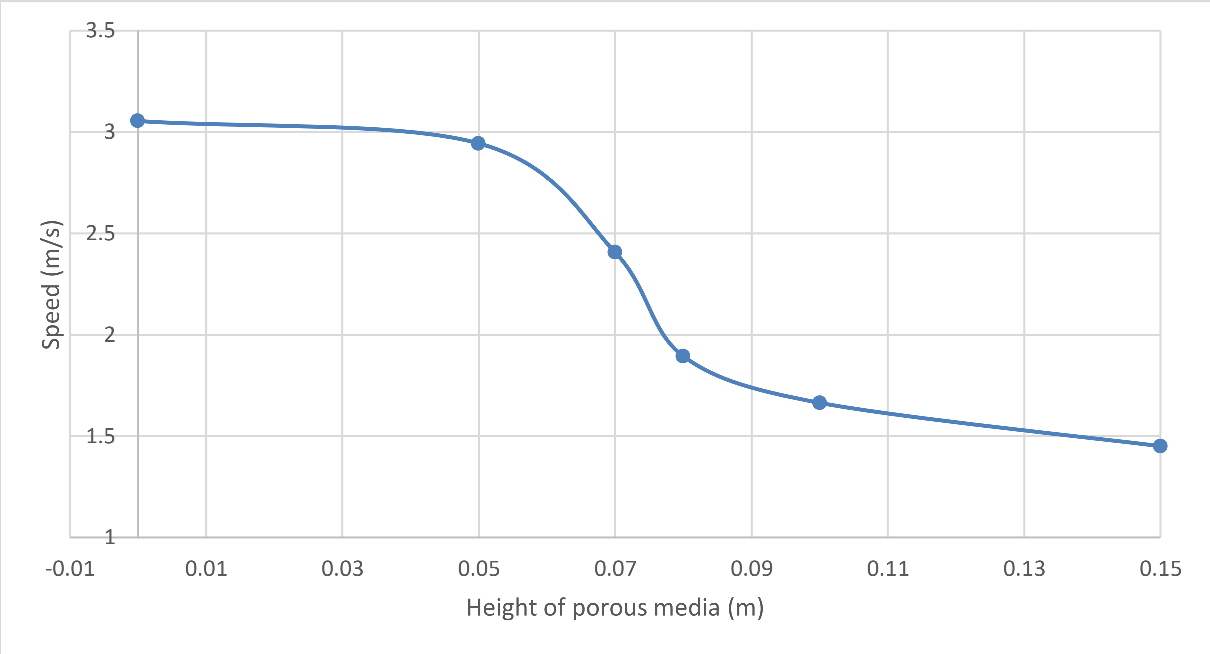

Figure 5.4 – The graph of the speed of water propagating through the porous media against the height of the porous media

5.3 EFFECT OF POROSITY ON FRONT FLOOD ON TWO DIFFERENT HEIGHT 0.07 M AND 0.15 M

5.3.1 Parameters

The heights of the porous media (H') used in this section are 0.07 m and 0.15 m. In addition, the values of porosity investigated are 0.50, 0.70, 0.80 and 0.95. The model without the porous media is also investigated to allow the comparison among the results.

5.3.2 Results

In Figure 5.5, both (a) and (b) illustrate similar results which means they agree with each other in terms of the effect of porosity (n) on the water wave propagation through the porous media. For n of 0.95, the behaviour of water propagating through the media is considered to be close to that of water travelling without any barrier. This means that it is easier for water to travel through in the porous media with the greater value of porosity which agrees with the fundamental principles. This is confirmed by other values of porosity as well since the lower porosity the porous media is, the easier the water can propagate through the media. This also shows that the media slow down the water when it attempts to travel through the porous structure.

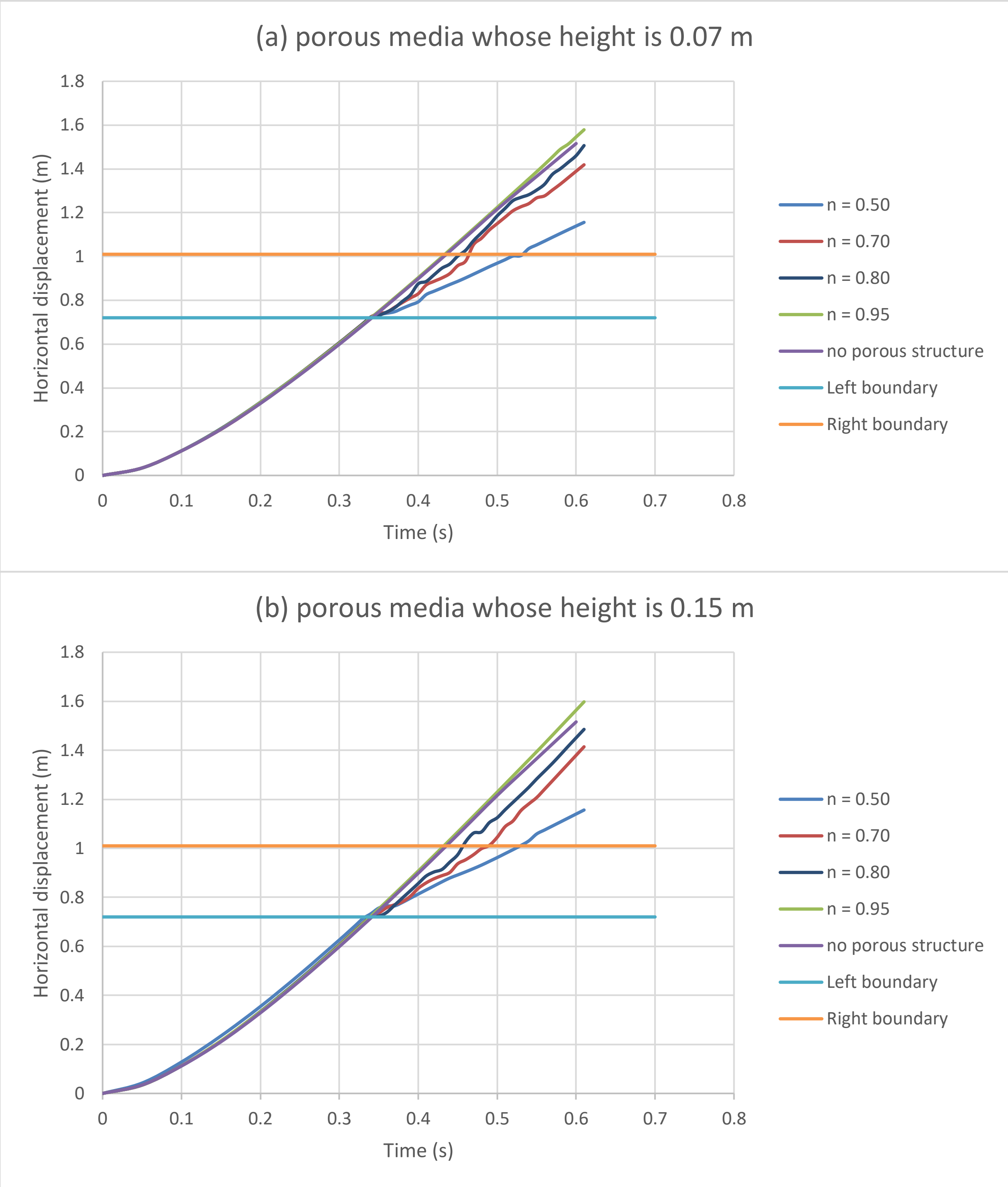

Figure 5.5 – The graph of the front flood position (x) against time for different porosity values: (a) for 0.07 m of porous media and (b) for 0.15 m of porous media

Time (s)	Height of 0.07 m	Height of 0.15m
0		
0.20		
0.35	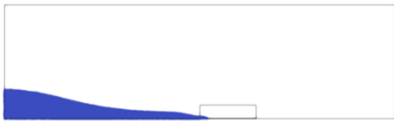	
0.40		
0.45	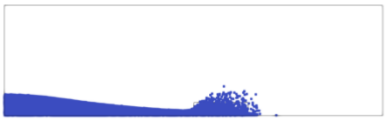	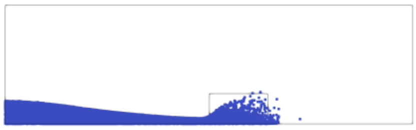
0.50	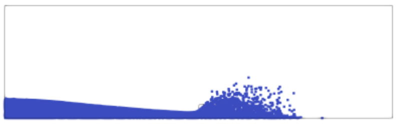	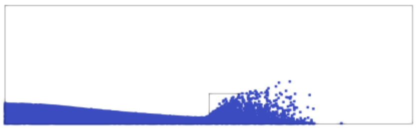
0.55	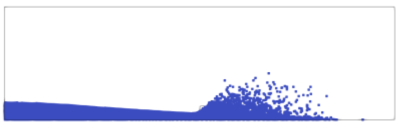	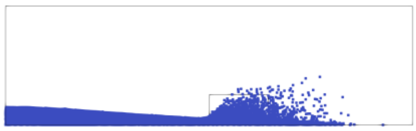
0.60	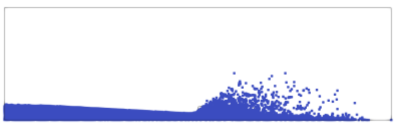	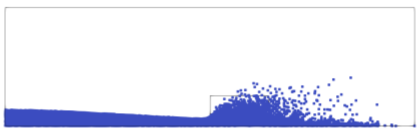

Figure 5.6 - Comparison of the results produce by MPM (on the left height of 0.05 m, on the right height of 0.15m) for the porosity of 0.70

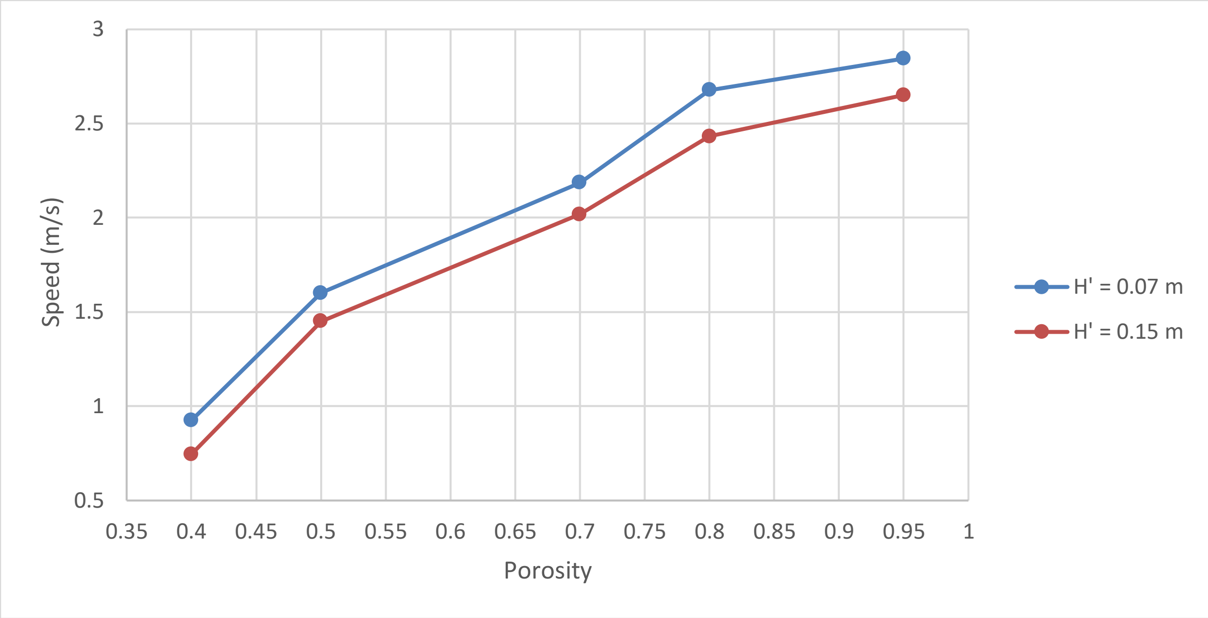

Figure 5.7 – The graph of the speed of water propagating through the porous media against porosity of porous media

In Figure 5.7, it can be seen that the water propagates through the $\mathrm{H}' = 0.15$ m media easier ($\mathrm{n} = 1$ is when there is no porous media in the flume). The trends between the two lines are similar to each other. This means that the value of porosity has impacted on the water speed through the porous structure. In addition, from Figure 5.6, there is a comparison of water propagation through the porous structure having $\mathrm{n} = 0.70$ between $\mathrm{H}' = 0.07$ m and $\mathrm{H}' = 0.15$ m. It is shown that even though the height of the porous media is different, the pattern of water propagation is similar to each other.

5.4 EFFECT OF GRAIN SIZE ON FRONT FLOOD ON TWO DIFFERENT HEIGHT 0.07 M AND 0.15 M

5.4.1 Parameters

The heights of the porous media (H') investigated in this section are 0.07 m and 0.15 m. In addition, the grain sizes (D) investigated in this section are 5 mm, 10 mm, 30 mm, 50 mm and 100 mm.

5.4.2 Results

In Figure 5.8, both (a) and (b) illustrate that the smaller grain size is, the more difficult water can travel through the porous structure. Therefore, those results agree with the fundamental principles. The behaviour of the water propagation having the grain size of 100 mm is similar to that without the porous media. The water behaviour of the media whose height is 0.15 m is closer to that of the media whose height is 0.07 m. This might be because there is overtopping in the media whose height is 0.07 m which has an impact on how fast water travels after the porous barrier.

In Figure 5.9, there is a comparison of water propagation through the porous media having the grain size of 30 mm between $\mathrm{H}' = 0.07$ m and $\mathrm{H}' = 0.15$ m. The overtopping water in the simulation of $\mathrm{H}' = 0.07$ m travels towards the right of the flume while that in the simulation of $\mathrm{H}' = 0.15$ m travels towards the left of the flume. This happens because the water particles can still travel through the media at $\mathrm{H}' = 0.15$ m so the bottom part of the overtopping can travel downwards and rightwards through the gaps within the media at the same time while the water particles cannot at $\mathrm{H}' = 0.07$ m so the overtopping part requires to travel through the right. For the 0.15m porous structure, the reflected water particles at the porous media wall is greater and travels back further when compared to those of the 0.07 m porous structure. This could mean that, with the same grain size particles within the porous structure, the higher porous structure could slow down a portion of water to travel pass through itself. Meanwhile, the scattered water particles from the collision with the porous media are around the porous media. However, the most of them is around the front flood position of the water travel path. The breakwater occurs within the porous media in both of the heights, while the water overtopping the barrier occurs only in the lower porous media.

In Figure 5.10, the trends between $\mathrm{H}' = 0.07$ m and $\mathrm{H}' = 0.15$ m are dissimilar. However, it is obvious that the larger the grain size is, the faster the water can travel through the porous media for each height. Between the grain size values of 23 mm and 65 mm, the speed of water propagating through the media of $\mathrm{H}' = 0.15$ m is greater than that of $\mathrm{H}' = 0.07$ m. This disagrees with section 5.2 where states that the greater height of the porous media gives a lower speed of water travelling through the porous barrier. However, the section 5.2 was investigated in one particular grain size which was 15.9 mm. This could mean that the lower water speed as the height of the barrier is higher is true in a certain value range of grain sizes. An alternative could be that there are critical grain size values that are exceptions to the aforementioned statement in the previous section 5.2. However, this only applies to this specific case that is investigated in this section 5.4.

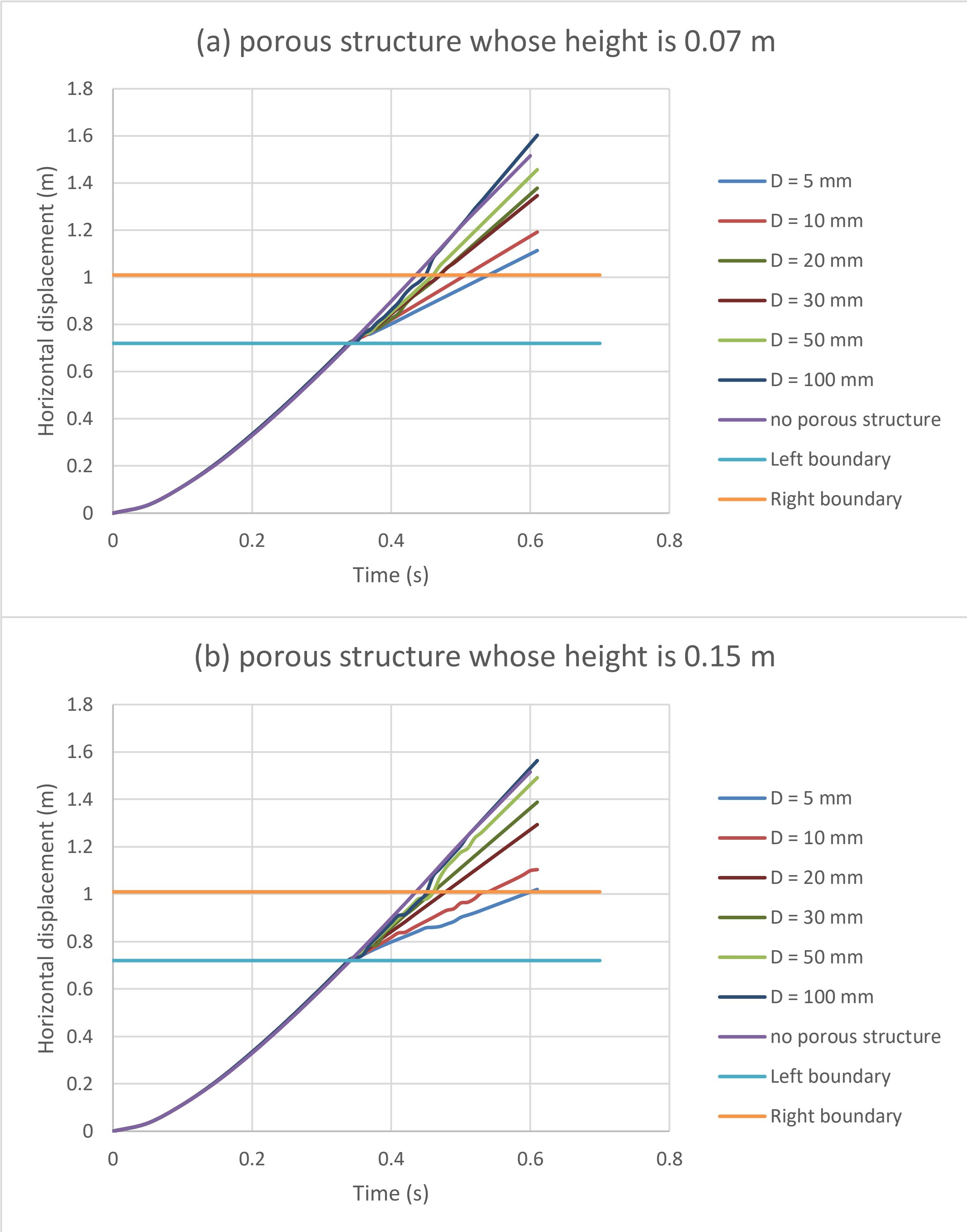

Figure 5.8 – The graph of the front flood position (x) against time for different grain size values: (a) for 0.07 m of porous media and (b) for 0.15 m of porous media

Time (s)	Height of 0.07 m	Height of 0.15m
0		
0.20		
0.35		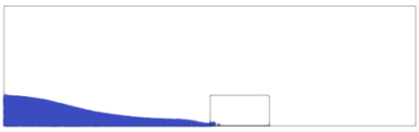
0.40	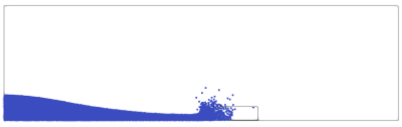	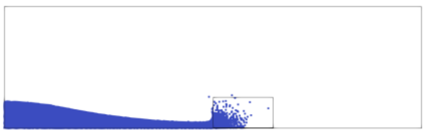
0.45	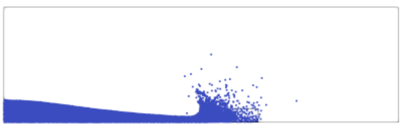	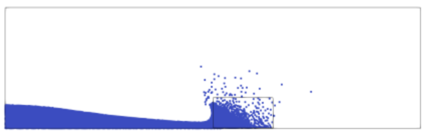
0.50	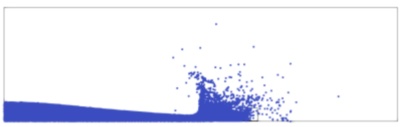	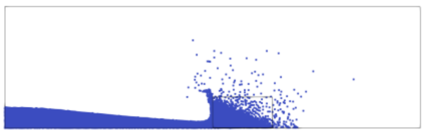
0.55	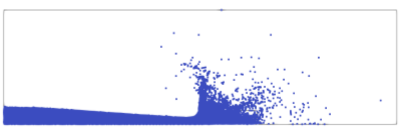	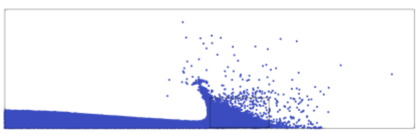
0.60	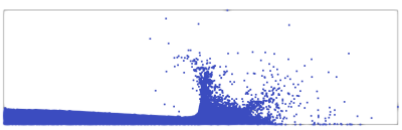	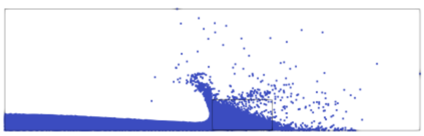

Figure 5.9 - Comparison of the results produce by MPM (on the left height of 0.05 m, on the right height of 0.15m) for the grain size of 30 mm

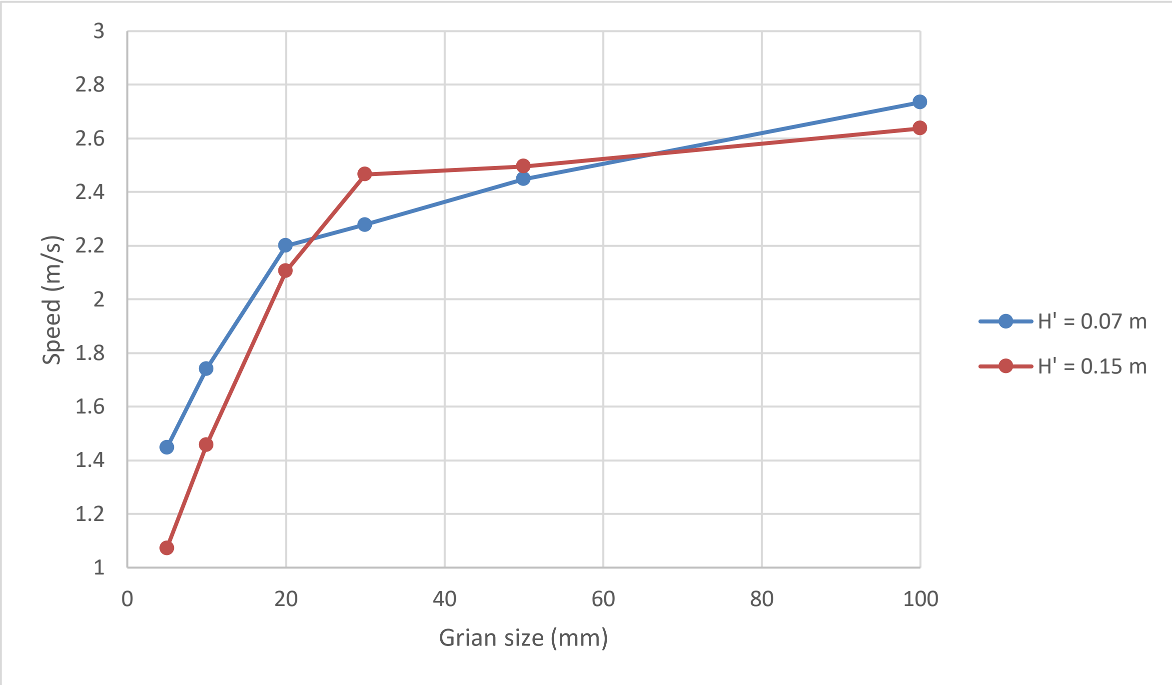

Figure 5.10 – The graph of the speed of water propagating through the porous media against the grain size of the porous media

Chapter 6: Conclusions

In this research, a porous media is investigated via two-point MPM. The capability of the porous media to absorb wave energy is an interest in coastal engineering. In addition, as the flow friction developing within the porous media can be exploited to create significant wave energy dissipation. In order to verify the accuracy of the MPM, simulations of dam-break flows are carried out and the results are in good agreement with other validated numerical methods and experimental data. Furthermore, simulations of the model from Liu et al.'s paper (1999) are investigated, and the results are also in good agreement with the experimental data obtained. Therefore, MPM is considered to be the most suitable method for this investigation.

There are three key factors related to the porous media that are investigated in this study (Height, Porosity and Grain size). In terms of height of the porous media (H'), it is shown that the taller the porous media is, the slower the water can travel through the barrier. The reasons to explain this phenomenon are, for example, there are more spaces within the structure that can contain more water particles, so the water particles take more time to travel to the other side of the porous structure when compared to the speed of the overtopping water and the amount of the reflected water at the barrier is greater with a higher media, thereby easing some portion of the water to reach the end of the flume. In addition, there are two distinct trends when the graph of the front flood position against time is considered (one is roughly parallel with the trend without porous structure and the other is not), so, for the next two factors, one height from each trend is investigated, $\mathrm{H}' = 0.07$ m and $\mathrm{H}' = 0.15$ m.

For the investigation of effect of porosity, there are four values included in the study which are 0.50, 0.70, 0.80 and 0.95 in both of the height. They both show that the greater value of porosity the porous barrier has, the faster the speed of water travels through the structure. Moreover, when consider the graph of speed of water propagating through the porous media against porosity value, it is demonstrated that both of the heights have similar trends.

In the study of impact of grain size, there are five values included in this investigation which are 5 mm, 10 mm, 30 mm, 50mm and 100mm in both of the heights. They both show that the greater value of grain size the porous barrier has, the faster the speed of water travels through the structure. This means that it is easier for water to travel through the porous media with a greater grain size since the total distance for water to travel is lower. When the graph of the speed of water propagating through the porous media against the grain size is deemed, there is no clear trend between those two height values. Between approximately 23 mm and 65 mm, the speed of water from $\mathrm{H}' = 0.15$ m is greater than that from $\mathrm{H}' = 0.07$ m. However, this exception might apply to only this model.

In terms of the further study, the wave column on the left-hand side of the flume can be changed into a set of stationary waves, which might produce more realistic results when compared to the real-world scenarios. Furthermore, by placing the porous media, it is on a small-angle slope would make it more realistic.

Bibliography

1. Abe, K., Soga, K. & Bandara, S. (2014) Material Point Method for coupled hydromechanical problems. *Journal of Geotechnical Engineering.* 140(3).
2. Altomare, C., Crespo, A., Rogers, B., Dominguez, J., Gironella, X. &Gómez-Gesterira, M. (2014). Numerical modelling of armour block sea breakwater with smoothed particles hydrodynamics. *Computers &Structures*. 130, 34-45.
3. Anderson, S. M. (2009) *Material-point analysis of large-strain problems: modelling of landslides*. PhD thesis, Aalborg University.
4. Bandara, S. &Soga K. (2015) Coupling of soil deformation and pore fluid flow using Material Point Method. *Computers and Geotechnics*. 63, 199-214.
5. Beuth, L., Benz, T., Vermeer, P. & Więckowski, Z. (2007) Large deformation analysis using a quasi-static Material Point Method. *Journal of Theoretical and Applied Mechanics*. 38, 45-60.
6. Brackbill, J. U., Kothe, D. B. & Ruppel, H.M. (1988) FLIP: a low-dissipation, particle-in-cell method for fluid flow. *Computer Physics Communications*. 48(1), 25-38.
7. Bullock, G., Obharai, C., Peregrine, D. & Bredmose, H. (2007) Violent breaking wave impacts. Part 1: Results from large-scale regular wave tests on vertical and sloping walls. *Coastal Engineering*. 54(8), 602-617.
8. Cummins, S. J. & Rudman, M. (1999) An SPH projection method. *Journal of Computational Physics*. 152(2), 584-607.
9. Danielson, F., Sørensen, M, K., Olwig, M. F., Selvan, V., Parish, F., Burgess, N, D., Hiraishi, T., Karunagaran, V, M., Rasmussen, M, S., Hansen, L, B., Quarto, A. & Suryadiputra, N. (2005) The Asia Tsunami: A Protective Role for Coastal Vegetation. *Science*. 310 (5748), 643.
10. Ergun, S. (1952). Fluid flow through packed columns, pages 89-94.
11. Fern, E.& Soga, K. (2016) The role of constitutive models in MPM simulations of granular column collapses. *Acta Geotechnica*. 11(3), 659-678.
12. Gui, Q., Dong. P., Shao, S. & Chen., Y. (2015) Incompressible SPH simulation of wave interaction with porous structure. *Ocean Engineering*. 110, 126-139.

13. Hadadpour, S., Paul, M. & Oumeraci., H. (2019) Numerical investigation of wave attenuation by rigid vegetation based on a porous media approach. Journal of Coastal Research. 92, 92-100.
14. Hattori, M., Arami, A. & Yui, T. (1994) Wave impact pressure on vertical walls under breaking waves of various types. *Coastal Engineering*. 22, 79-114.
15. Hirt, C. W.& Nichols, B. D. (1981) Volume of fluid (VOF) method for the dynamics of free boundaries. *Journal of Computational Physics*. 39(1), 201-205.
16. Huang, L.& Chao, H. (1992) Reflection and transmission of water wave by porous breakwater. *Journal of Waterway, Port, Coastal and Ocean Engineering.* 118(5), 437-452.
17. Hsu, T. -J., Sakakiyama, T.& Liu, P.L.-F. (2002) A numerical model for wave motions and turbulence flows in front of a composite breakwater. *Coastal Engineering*. 46(1), 25-50.
18. Iryanto, I.& Gunawan, P. H. (2016) Simulation of wave mitigation by coastal vegetation using smoothed particles hydrodynamics method. *Journal of Physics*: Conference Series, 693.
19. Jassim, I., Stolle, D. & Vermeer, P. (2013). Two-phase dynamic analysis by Material Point Method. *International Journal for Numerical and Analytical Methods in Geomechanics*. 37(15), 2502-2522.
20. Khayyer, A., Gotoh, H.& Shao, S. (2008) Corrected incompressible SPH method for accurate water-surface tracking in breaking waves. *Coastal Engineering*. 55(3), 236-250.
21. Khayyer, A., Gotoh, H.& Shao, S. (2009) Enhances predictions of wave impact pressure by improved incompressible SPH methods. Applied Ocean Research. 31(2), 111-131.
22. Khayyer, A., Gotoh, H., Simizu, Y., Gotoh, K.& Shao, S. (2017) An Enhanced Particles Method for Simulation of Fluid Flow Interactions with Saturated Porous Media. Journal of Japan Society of Civil Engineers, *Ser. B2(Coastal Engineering)*, 73(2).
23. Koraima, A., Heikal, E.& Zaid, A. A. (2014) Hydrodynamic characteristics of porous seawall protected by submerged breakwater. *Applied Ocean Research*. 46, 1-14.
24. Lean, G. H. (1967) A simplified theory of permeable wave absorbers. *Journal of Hydraulic Research*. 5(1), 15-30.

25. Li, Y., and Raichlen, F. (2001) Solitary wave runup on plane slopes. *Journal of Waterway, Port, Coastal and Ocean*, 127: 33-44.
26. Liang, D. (2009) Evaluating shallow water assumptions in dam-break flows. *Proceedings of the Institution of Civil Engineers- Water management*, 163: 227-237.
27. Liang, D., Jian, W., Shao, S., Chen, R.& Yang., K. (2017) Incompressible SPH simulation of solitary wave interaction with movable seawalls. Journal of Fluids and Structures. 69, 72-88.
28. Liu, P. -F., Lin, P., Change, K. -A.& Sakakiyama, T. (1999) Numerical modelling of wave interaction with porous structures. *Journal of Waterway, Port, Coastal and Ocean Engineering*. 125(6), 322-330.
29. Martin, J. C.& Moyce, W. J. (1952) An experimental study of the collapse of liquid columns on a rigid horizontal plane. Philosophical Transactions of the Royal Society of London Series A. 244(88), 312-324.
30. Monagham, J.& Kos, A. (1999) Solitary waves on a Cretan beach. *Journal of Waterway, Port Coastal and Ocean Engineering*. 125(3), 145-154.
31. Monaghan, J. J. (1992) Smoothed Particle Hydrodynamics. *Annual Review of Astronomy and Astrophysics*. 30, 543-574.
32. Monaghan, J. J. (1994) Simulating free surface flows with SPH. *Journal of Computational Physics*. 110, 399-406.
33. MPM Research Community (2019). *Anura3D MPM Software Scientific Manual Version 2019.1- Tinctorius*. Anura3D MPM Research Community.
34. NOAA (National oceanic and atmospheric administration). (January 2017) Global and regional sea level rise scenarios for the United States. *NOAA Technical Report NOS COCPS 083*.
35. Ogolo, N., Akinboro, O., Inam, J., A.F.& Onyekonwu, M. (2015) Effect of grain size on porosity revisited. SPE Nigeria Annual International Conference and Exhibition.
36. Ren, B., Wen, H., Dong, P.& Wang, Y. (2016) Improved SPH simulation of wave motions and turbulent flows through porous media. *Coastal Engineering*. 107, 14-27.
37. Rogers, B. D., Dalrymple, R. A., and Stansby, P. K. (2009) Simulation of caisson breakwater movement using 2D SPH. *Journal of Hydraulic Research*, 48: 135-141.
38. Sakakiyama, T., and Liu, P. L. F (2001). Laboratory experiments for wave motions and turbulence flows in front of a breakwater. *Coastal Engineering*, 117-139.
39. Savage, R. P., and Fairchild, J. C. (1953) Laboratory study of wave energy losses by bottom friction and percolation. *Coastal Engineering research Centre*, Vicksburg.

40. Shao, S. and Lo, E. Y. (2003) Incompressible SPH flow model for wave interactions with porous media. *Coastal Engineering*, 57(3): 304-316.

41. Straub, L., Bowers, C., and Herbick, J. (1957) Laboratory studies of permeable wave absorbers. Proceedings of 6th Conference on Coastal Engineering, 729-742.

42. Sulisz, W. (1985) Wave reflection and transmission at permeable breakwaters of arbitrary cross-section. Coastal Engineering, 9(4): 371-386.

43. Sulsky, D., Chen, Z., and Schreyer, H. (1994) A particle method for history-dependent materials. Computer Methods in Applied Mechanics and Engineering, 118: 179-196.

44. Sulsky, D., Zhou, D, J., and Schreyer, H, L. (1995) Application of particle-in-cell method to solid mechanics. Computer Physics Communications, 87: 236-252.

45. van der Meer, J. M., Stolle, D., and Jassim, I. (1992) Runup on smooth and rocks slopes of coastal structures. *Journal of Waterway, Port, Coastal and Ocean Engineering*, 118: 543-550.

46. Yerro, A., Alonso, E. E., and Pinyol, N. (2015) The Material Point Method for unsaturated soil. *Géotechnique*, 65(3): 201–217

47. Zhao, X., and Liang, D. (June 2016) MPM modelling of seepage flow through embankments. International Society of Offshore and Polar Engineers.

48. Zhao, X., Liang, D., and Martinelli, M. (2017) MPM simulations of dam-break floods. Journal of Hydrodynamics. Ser. B, 29(3): 397-404.

Appendices

Appendix A

Risk Assessment

The risk assessment submitted to the Safety Office at the start of Michaelmas term 2019 is attached below. In retrospect, the form accurately reflects the hazards encountered during the project. As this was a project based on running computer simulations, the risks would likely not have been evaluated differently if starting the project again.

More care should be taken with the use of the guidance on working with display screen equipment.

Appendix B

Covid-19 disruption

When the department was shut down, the computer in the lab was not accessible due to a disruption in the remote access. After approximately two weeks, we could create a new connection to remotely access the computer to run the simulations.

Moreover, I self-isolated for a week due to a presence of high fever. In addition, during this pandemic, my mental health was not in a good state. I was far away from my loved ones which was one of many factors causing issues in my mental health. The Thai government declared the emergency decree to permit any flight to enter the Kingdom of Thailand which was extended until 30th June 2020. Therefore, I could not go back to my home during this crisis which definitely affects negatively on my ability to work and therefore my performance.